Observation of solvatochromism in CdSe colloidal quantum dots

C. A. Leatherdale and M. G. Bawendi*
Department of Chemistry and Center for Materials Science and Engineering, Massachusetts Institute of Technology, 77 Massachusetts Avenue, Cambridge, Massachusetts 02139

(Received 13 June 2000; revised manuscript received 1 December 2000; published 4 April 2001)

We report solvatochromatic shifts in the absorption spectra of colloidal CdSe quantum dots that are consistent with the change in polarization energy of the quantum-confined exciton. Good agreement with theory is found when the screening from the ligand shell is included. The polarization energy also accounts for the spectral shift between dilute dispersions and close-packed quantum dot solids. Experiments with pure and mixed-size quantum dot solids suggest that solvatochromism dominates the redshift observed with quantum dot (2–6-nm diameter) solids.

DOI: 10.1103/PhysRevB.63.165315 PACS number(s): 77.22.−d, 73.21.−b, 31.70.Dk

I. INTRODUCTION

Semiconductor quantum dots (QD's) are of interest as model systems to study the transition from molecular to bulklike material properties.[1,2] As well, a variety of device applications[3] have been proposed including photovoltaics,[4,5] flash memory,[6] and single-photon detectors.[7] Efficient operation of many of these devices as well as interpretation of single-charge tunneling spectra[8] requires a detailed understanding of the energy required to add or to remove a charge from the QD. For semiconductor QD's, the charging energy depends on both the direct Coulomb interaction of charges confined to QD and the polarization energy due to the dielectric environment.[9] Numerous theoretical papers have presented calculations of the polarization energy as a function of QD size[9–15] and shape.[16] In addition, the dielectric environment may be important in the presence or absence of surface states.[17,18] However, these effects have not been studied experimentally until now.

Since they may be easily dispersed in a variety of solvents with different dielectric constants, colloidal semiconductor QD's are a convenient system in which to test theoretical models of the polarization energy. The QD optical band gap is predicted to depend weakly on the dielectric environment through interaction of the exciton with the same surface polarization charge that affects the charging energy.[11] In molecules, the analogous effect is known as solvatochromism and arises from dipole-(induced) dipole or dispersion interactions with the solvent molecules.[19,20] In this article, we show that the optical band gap of colloidal CdSe QD's is less sensitive to the dielectric environment than predicted from currently available models unless screening from the ligand shell is taken into account.

These measurements also allow us to address the important question of interdot coupling in close-packed arrays of semiconductor QD's. Optical absorption measurements are commonly used as a probe of interparticle coupling. In practice, changes in the absorption spectrum may be due to the dielectric environment, classical electromagnetic dipole or multipole coupling, or quantum-mechanical coupling (i.e., the wave function is delocalized over more than one QD to form extended states). For example, when gold nanoparticles aggregate, electromagnetic coupling of the plasmon resonances on nearby particles results in a dramatic color change[21] that can be used in colorimetric based detection schemes for nanoparticle tagged biomolecules.[22] Several authors have observed redshifts of the absorption edge when close-packed films of colloidal semiconductor QD's are prepared.[23,24] For very small clusters, it has been suggested that the redshift is due to quantum-mechanical coupling of adjacent QD's.[25] We examine this hypothesis by comparing the absorption shifts of monodisperse and mixed-size QD solids. Our analysis suggests that for larger clusters (2–6-nm diameter) the absorption shift is dominated by the effect of the external dielectric environment.

II. EXPERIMENT

CdSe QD's passivated by tri-octylphosphine/tri-octylphosphine oxide (TOP/TOPO) ligands are prepared following the method of Murray, Norris, and Bawendi.[26] QD's are isolated from the excess TOPO/TOP by repeated (3×) size selection from *n*-butanol/methanol dispersions followed by drying under vacuum. To form close-packed QD solids, concentrated dispersions (~100 mg/ml) of QD's in 90% hexane/10% octane are drop cast on clean microscope slides to form optically clear and thin films. Tri-butylphosphine/tri-butylphosphine oxide (TBPO/TBP) passivated QD's are prepared by repeated (2×) dissolution in neat TBPO/TBP and stirring overnight at 60 °C. QD radii[26] and interparticle separation[27] in QD solids are quoted from previously published results.

Linear absorption spectra are obtained using a Cary 5E uv–visible–near-infrared scanning spectrophotometer operating in dual-beam mode with 2-nm spectral bandwidth and sampling every 0.1 nm. Solution spectra are obtained using the same quartz cuvette for both reference and sample. For each sample, an aliquot of the stock dispersion is dried under vacuum to a powder and then redispersed in the new solvent, taking care to ensure that the QD's redisperse fully. Spectra for close-packed films are obtained using microscope slides as substrates. Error from the fluorescence of the QD's is minimized by washing the QD's with methanol several times to remove the excess capping ligands and reduce the photoluminescence quantum yield to ~1%. Photoluminescence

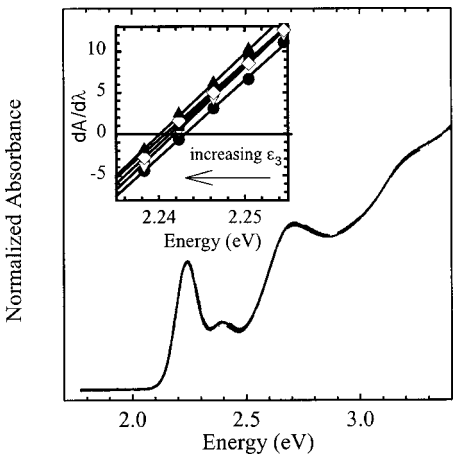

FIG. 1. Room-temperature linear absorption spectra for 20-Å TBPO/TBP capped CdSe QD's dispersed in various solvents. The inset shows the first derivative spectra in the region of the lowest energy absorption feature in hexane (●), chloroform (▽), toluene (■), 3-bromotoluene (◇), and 3-iodotoluene (▲). The zero crossing moves to lower energies with increasing solvent dielectric constant.

quantum yield measurements are made using a SPEX Fluorolog spectrophotometer.

III. RESULTS

Figure 1 shows linear absorption spectra for 20-Å radius CdSe QD's with TBPO/TBP surface ligands dispersed in hexane, chloroform, toluene, 3-bromotoluene, and 3-iodotoluene (all solvents from Aldrich, >98% purity). Each dispersion has an identical nominal concentration of QD's and is optically clear. Within our experimental error, there is no change in the extinction coefficient of the QD's. A slight redshift of the absorption edge is observed with increasing solvent refractive index. The shift in the first absorption feature ($1S_e1S_{3/2h}$ transition[28]) is more easily observed by plotting the derivative spectra (inset of Fig. 1) and fitting a straight line to the data near the zero crossing (peak maxima). The higher-energy optical transitions and the band edge photoluminescence (PL) also redshift by approximately the same amount as the $1S_e1S_{3/2h}$ transition. However, since perturbation theory limits our quantitative analysis of the polarization energy to the lowest excited state; from this point forward we concentrate on the $1S_e1S_{3/2h}$ transition.

In Fig. 2, we plot the energy difference between QD's dispersed in 3-iodotoluene and QD's in hexane for a size series of TOPO/TOP capped QD's. The shift in the $1S_e1S_{3/2h}$ transition is larger for small QD's (15–20 Å) than for large QD's (30–40 Å). This is expected as the quantum-confined exciton of smaller QD's is now on average closer to the surface polarization charge and the solvent molecules. We observe that changing the alkane chain length (and effectively the distance of closest approach of the solvent molecules to the QD surface) does not change the solvatochromatic shift significantly. Figure 3 shows data for 20-Å TOPO/TOP and TBPO/TBP capped QD's dispersed in the same solvent series as above (eight and four carbon chains,

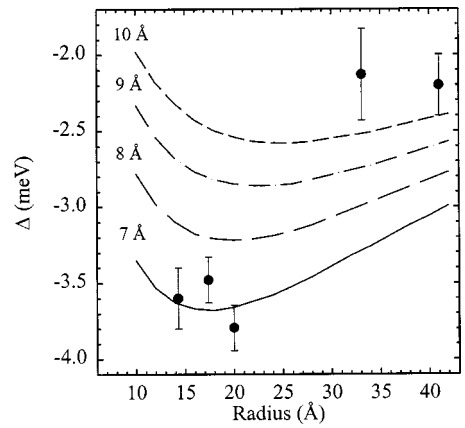

FIG. 2. Observed and predicted solvatochromatic shifts as a function of QD size. Symbols are the observed solvatochromatic shift between hexane and 3-iodotoluene dispersion. Theoretical predictions based on the inorganic-core–organic-shell model are shown for various shell thicknesses with dielectric constant $\varepsilon_2 = 2.1$.

respectively). The theoretical fits in Fig. 3 will be discussed in Sec. IV.

By preparing close-packed solids of QD's one can further increase the external dielectric constant around the QD's. Figure 4 shows the reversible absorption shift between a hexane dispersion and a close-packed film for 20-Å QD's with TOPO/TOP ligands. Each quantum-confined exciton is now effectively embedded in a matrix of CdSe and organic material. To determine the contribution of interdot coupling to the absorption shift, we prepare 1:10 mixtures of large (24-Å) QD's and small (13-Å QD's) and measure the absorption shift with respect to a pure dispersion of the large QD's. If

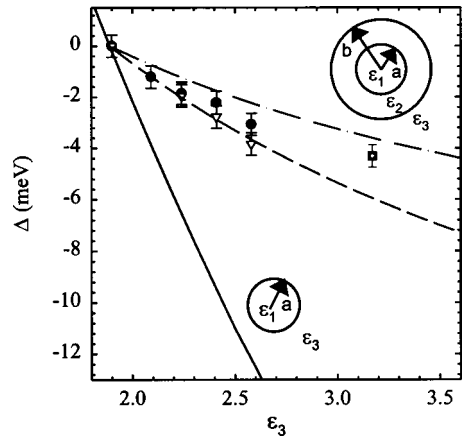

FIG. 3. Observed and predicted solvatochromatic shifts with respect to hexane dispersion for the $1S_e1S_{3/2h}$ electronic transition. Symbols are the observed shifts for 20-Å QD's capped with (▽) TOPO/TOP ligands and (●) TBPO/TBP ligands. The observed shift for a close-packed solid of approximately the same size QD's is shown by the square (■). The solid line is the theoretical shift for this core radius based on Eqs. (3)–(5). The predicted solvatochromatic shift using the core-shell model [Eqs. (5) and (6)] is shown for 7-Å (dashed) and 11-Å (dash-dotted) dielectric shells ($\varepsilon_2 = 2.1$) surrounding each QD.

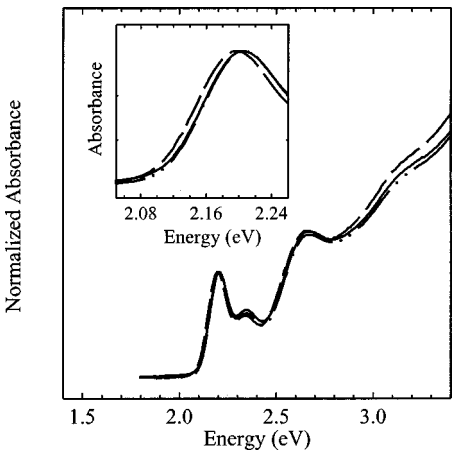

FIG. 4. Room-temperature linear absorption spectra for 20-Å TOPO/TOP capped QD's as a dispersion in hexane (solid lines), a close-packed QD solid on glass (dashed line), and the same QD's redispersed in hexane (dash-dot-dotted line).

coupling of adjacent QD electronic states is the dominant contribution to the observed shift, then the $1S_e1S_{3/2h}$ transition of the large QD's should not shift in the mixed QD system. Kagan, Murray, and Bawendi showed that the different-size QD's remain well mixed and do not phase-separate when deposited from hexane/octane solution.[29]

Typical spectra for the mixed QD's are shown in Fig. 5. The simulated mixed spectrum (-▽-) is determined by measuring the absorption spectra for the pure QD solids or dispersions and then adding these spectra in the appropriate ratio to best match the observed, mixed, spectrum (solid line). Panel B of Fig. 5 shows that a linear combination of the individual spectra reproduces the energy but not the precise absorbance of the large QD's. The uncertainty in the peak energy is estimated at ±0.1 nm. Table I summarizes the observed and predicted energy of the $1S_e1S_{3/2h}$ transition for both the mixed dispersions and mixed QD solids.

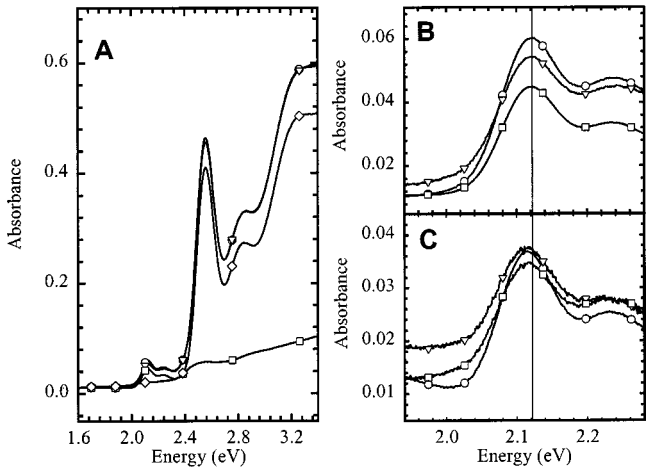

FIG. 5. (A) Room-temperature linear absorption spectra of dilute dispersions of pure and mixed QD's for 24-Å QD's (□), 13-Å QD's (◇), a 1:10 mixture (○), and the best fit, linear combination of the large and small QD spectra (▽). (B) Enlargement of the spectra near the band edge for dispersions of large QD's both when monodisperse and when mixed with the small QD's. (C) Same as (B) but for close-packed films of QD's. The reference line indicates the energy of the $1S_e1S_{3/2h}$ transition for a pure dispersion of the large QD's.

TABLE I. Observed and predicted position of the first absorption feature for 24-Å QD's as pure dispersions and close-packed solids, and when mixed with 13-Å QD's. The uncertainty is estimated at ±0.1 nm.

Sample	Observed (nm)	Predicted (nm)
Large QD dispersion	584.3	
Large QD solid	585.4	585.3[a]
Mixed QD dispersion	584.0	584.1[b]
Mixed QD solid	585.8	585.7[c]
		584.9[d]
		586.2[e]

[a]Core-shell model ($b-a=9$ Å, $\varepsilon_{av}=2.84$).

[b]Predicted peak position for spectra=10×(small QD dispersion) +1×(large QD dispersion).

[c]Mixed dispersion position+shift based on the core-shell model, $\varepsilon_{av}=2.58$, $b-a=9$ Å.

[d]Predicted peak position for spectra=$A\times$(small QD solid)+B ×(large QD dispersion).

[e]Predicted peak position for spectra=$A\times$(small QD solid)+B ×(large QD solid).

We simulate the $1S_e1S_{3/2h}$ transition energy of the large QD's in the mixed QD solid assuming several different scenarios. One possibility is that there is no change in the transition energy of the large QD's and thus the total absorption spectrum is the sum of the small QD solid spectrum plus the large QD dispersion spectrum (footnote d). Table I shows that this senario overestimates the $1S_e1S_{3/2h}$ transition evergy of the large QD's. A second possibility is that the mixed QD solid spectrum is a linear combination of the small and large QD *solid* spectra (footnote c). This scenario slightly underestimates the large QD $1S_e1S_{3/2h}$ transition energy. The cases indicated by footnotes a and c are discussed in Sec. IV.

Before proceeding to a detailed analysis of the effect of the dielectric environment, it is important to eliminate other effects that could be causing spurious changes in the absorption spectra. Even for nearly monodisperse QD's, as used in this experiment, the remnant size distribution still affects the shape and energy of the absorption spectrum. If varying solubility of the QD's was causing the absorption shifts, we would expect that with increasing solvent polarity, the largest particles would flocculate first (strongest van der Waals interactions), leading to a blueshift of the absorption spectrum. This is not observed. Furthermore, all the dispersions were optically clear (optical density <0.01 below the band gap), suggesting aggregation is not making a significant contribution. Thus we assign the redshift of the absorption spectrum to changes in the dielectric environment that perturb the energy of the quantum-confined exciton.

IV. DISCUSSION

In the strong quantum-confinement regime, the dependence of the optical band gap on the dielectric environment

is generally calculated using the effective-mass approximation, assuming an infinite potential barrier at the boundary, and applying perturbation theory to account for the potential from the image charge.[11,12,14] We will show that this simple approach overestimates the effect of changing the solvent environment around colloidal QD's. However, with a straightforward modification of the potential to account for the presence of the ligand shell, good agreement is possible.

The total energy of an exciton confined to a spherical semiconductor QD is the sum of the bulk band gap, the kinetic energy of each carrier due to quantum confinement, the energy from the direct Coulomb interaction of the electron-hole pair, the self-charging energy for each carrier ($\Sigma^{\mathrm{pol}}_{e(h)}$), and the polarization energy from the interaction of each carrier with the image charge of the opposite carrier ($J^{\mathrm{pol}}_{e,h}$):

$$E^{\mathrm{opt}}_{\mathrm{gap}}=E^{\mathrm{bulk}}_{g}+E^{\mathrm{kin}}_{e}+E^{\mathrm{kin}}_{h}+E^{\mathrm{dir}}_{\mathrm{Coul}}+\sum_{h}^{\mathrm{pol}}+\sum_{e}^{\mathrm{pol}}+J^{\mathrm{pol}}_{e,h}. \quad (1)$$

The first four terms depend only on the dielectric constant inside the QD (ε_1). The latter three polarization terms depend strongly on the contrast between the internal and external dielectric environment (ε_3). In the presence of an electric field, dielectric mismatch results in a surface polarization charge at the interface that interacts with charges confined within the QD. With an infinite potential barrier at the boundary, the lowest energy envelope wavefunction in a QD of radius a is proportional to $\sin(\pi r/a)/r$.

The self-energy $\Sigma^{\mathrm{pol}}_{e(h)}$ due to the image charge distribution on the surface when a hole (electron) is added to the highest valence (lowest conduction) band state is given by $\Sigma^{\mathrm{pol}}_{h(e)}=\frac{1}{2}\langle\Psi_0|V_{\mathrm{in}}(r,r')|\Psi_0\rangle$, where V_{in} is the polarization potential created by the image charge. For the case treated theoretically by Brus[11] and others,[12,14] the indirect polarization potential at point r, created by a point charge q at position r' within a spherical region is given by

$$V_{\mathrm{in}}(r,r')=\frac{q}{4\pi\varepsilon_0\varepsilon_1}\sum_{l=0}^{\infty}A_l r^l r'^l P_L(\cos\theta), \quad (2)$$

where P_L is the Legendre polynomial, θ is the angle between r and r', and ε_0 is the permittivity of free space. For the case where the image charge is at the interface between regions I and III (see circle in Fig. 3), the coefficient A_1 is given by

$$A_l=\frac{(l+1)}{a^{2l+1}}\frac{\varepsilon_1-\varepsilon_3}{\varepsilon_3+l(\varepsilon_1+\varepsilon_3)}. \quad (3)$$

From Ref. 12, $J^{\mathrm{pol}}_{e,h}$ is given by

$$J^{\mathrm{pol}}_{e,h}=\int\int\Psi_e(r')\Psi_h(r')V_{\mathrm{in}}(r,r')\Psi_e(r)\Psi_h(r)dr'dr$$
$$=\frac{-q^2}{4\pi\varepsilon_0\varepsilon_1 a}\left(\frac{1}{\varepsilon_3}-\frac{1}{\varepsilon_1}\right). \quad (4)$$

Allan *et al.* showed that the $l=0$ terms in $\Sigma^{\mathrm{pol}}_{e}$ and $\Sigma^{\mathrm{pol}}_{h}$ exactly cancel $J^{\mathrm{pol}}_{e,h}$ so that the net correction to the $1S_e1S_h$ exciton energy from the interaction with the image charge is given by[14]

$$\delta=\frac{\pi q^2}{2\varepsilon_0\varepsilon_1 a}\sum_{l=1}^{\infty}a^{2l+1}A_l\int_0^l j_0^2(\pi x)x^{2l+2}dx, \quad (5)$$

where j_0 is the spherical Bessel function.

Iwamatsu *et al.* considered the effect of a dielectric discontinuity for the case of a spherical QD surrounded by a shell of a second material with dielectric constant ε_2 and thickness $(b-a)$ (see inset of Fig. 3) and then embedded in a dielectric medium (ε_3).[15] In this case A_1 is given by

$$A_l=\frac{(l+1)}{a^{2l+1}}\frac{a^{2l+1}(\varepsilon_2-\varepsilon_3)[\varepsilon_1+l(\varepsilon_1+\varepsilon_2)]+b^{2l+1}(\varepsilon_1-\varepsilon_2)[\varepsilon_3+l(\varepsilon_2+\varepsilon_3)]}{a^{2l+1}(\varepsilon_1-\varepsilon_2)(\varepsilon_2-\varepsilon_3)l(l+1)+b^{2l+1}[\varepsilon_2+l(\varepsilon_1+\varepsilon_2)][\varepsilon_3+l(\varepsilon_2+\varepsilon_3)]}. \quad (6)$$

The rest of the derivation of the polarization energy follows as before, including the cancellation of the $l=0$ terms so that the correction to the exciton energy is given by Eq. (5) and substituting Eq. (6) for A_l.

In Fig. 3, we plot the energy of the first absorption feature from the data in Fig. 1 with respect to the value for the same QD's dispersed in hexane (Δ) versus the square of the solvent refractive index.[30] The dashed line shows the predicted energy shift based on Eqs. (3)–(5), where the image charge is considered to be exactly at the surface of the QD and using the bulk dielectric constant for CdSe ($\varepsilon_1=6.2$). The predicted energy shift is much larger than what it is observed. Using this model, it is not possible to match the data without assuming an unphysically large radius ($\sim 4a$). The solid line in Fig. 3 is the theoretically predicted energy shift with respect to hexane dispersion using the core-shell model [Eqs. (5) and (6)] and again using $\varepsilon_1=6.2$. Although there is no unique fit based on both shell thickness and ε_2, we can choose a physical solution by setting ε_2 equal to the dielectric constant of the ligand shell that surrounds each QD. Good agreement with the data is found setting the shell dielectric constant $\varepsilon_2=2.1$ and using the shell thickness b as the only fit parameter.[32] For the best fit, we find that the shell thickness is ~8 Å in reasonable agreement with the extended chain length for TBPO (~6.7 Å). The apparent shell thickness is insensitive to the value chosen for ε_2 over the range $1.9<\varepsilon_2<2.2$ (reasonable values for alkanelike molecules).

In Fig. 3 we also include the observed absorption shift for a QD solid (shown by the square) of similar size as used for

the solvent series. Here ε_3 is calculated for randomly close-packed spheres (fill factor$=0.64$) of semiconductor ($\varepsilon=6.2$ for bulk CdSe) with an organic shell of width (d) and dielectric constant $\varepsilon\sim 2$ and interstices filled with the same organic material. The observed absorption shift is in near quantitative agreement with what would be expected from the average external dielectric environment using the inorganic-core–organic-shell model. The data in Table I also show remarkably good agreement with this model. The $1S_e1S_{3/2h}$ transition for the large QD's shifts to the red with respect to hexane dispersion both for the monodisperse QD solid and when the QD's are ''diluted'' in a solid of small QD's. In the latter case, there should be little coupling between electronic states on adjacent QD's. The case for footnote a in Table I is the predicted $1S_e1S_{3/2h}$ peak position in the QD solid for monodisperse 24-Å QD's when ε_3 is the volume weighted, average dielectric constant of the composite (b-$a=9$ Å). When the large QD's are diluted in the small QD's, the volume fraction of semiconductor material is smaller, leading to a reduced average dielectric constant and correspondingly smaller absorption shift (case for footnote c).

The inorganic-core–organic-shell model is physically consistent with the monolayer of phospho-alkane ligands that surround each QD and provide a barrier to solvent molecules approaching the surface. In solvatochromism of molecular species, it is found that 90% of the solute-solvent interaction is with the first solvent shell.[19] Thus it is reasonable that the QD-ligand shell interaction dominates what it is observed. We observe that QD's capped with the eight and four carbon chain ligands exhibit the same solvatochromatic shifts within experimental error (Fig. 3). This result is not inconsistent with the core-shell model since the degree of penetration of solvent molecules into the ligand shell should depend on QD core size and ligand chain length as well as chemical and steric interactions with the solvent molecules.[31] When the radius of curvature of the particle is lower (larger QD's), increased surface coverage by the capping ligands is possible and the shell may be more impenetrable to the solvent. The solvatochromatic shifts for the large radius particles (30–40 Å) are more consistent with a 10–11-Å shell than for the 15–20-Å particles, which are consistent with an 8-Å dielectric shell (see fits in Fig. 2).

V. CONCLUSIONS

Solvatochromatic shifts are observed for CdSe colloidal QD's that are consistent with the change in polarization energy of the quantum-confined exciton. The ligand shell appears to partially insulate the semiconductor core from interactions with external environment. The observation of an absorption shift in the mixed QD system and the excellent agreement with the solvatochromatic core-shell model make a convincing argument that for QD's in this size range, the absorption shifts from dilute dispersion to close-packed film are dominated by the change in dielectric environment.

ACKNOWLEDGMENTS

The absorption measurements were made at the MIT Center for Materials Science Spectroscopy Laboratory. C.A.L. would like to thank NSERC, Canada for financial support. This work was supported primarily by the MRSEC Program of the National Science Foundation under award number DMR 98-08941.

*Author to whom correspondence should be addressed: 77 Massachusetts Avenue, Room 6-223, Cambridge, MA 02139. Email: mgb@mit.edu

[1] A. P. Alivisatos, Science **271**, 933 (1996).
[2] For an introduction to semiconductor QD's see U. Woggon, *Optical Properties of Semiconductor Quantum Dots* (Springer, New York, 1997), and references therein.
[3] K. K. Likharev, Proc. IEEE **87**, 606 (1999).
[4] N. C. Greenham, X. G. Peng, and A. P. Alivisatos, Phys. Rev. B **54**, 17 628 (1996).
[5] W. U. Huynh, X. Peng, and A. P. Alivisatos, Adv. Mater. **11**, 923 (1999).
[6] J. J. Welser, S. Tiwari, S. Rishton, K. Y. Lee, and Y. Lee, IEEE Electron Device Lett. **18**, 278 (1997).
[7] S. Komiyama, O. Astafiev, V. Antonov, T. Kutsuwa, and H. Hirai, Nature (London) **403**, 405 (2000).
[8] U. Banin, Y. W. Cao, D. Katz, and O. Millo, Nature (London) **400**, 542 (1999).
[9] A. Franceschetti and A. Zunger, Phys. Rev. B **62**, 2614 (2000).
[10] L. E. Brus, J. Chem. Phys. **79**, 5566 (1983).
[11] L. E. Brus, J. Chem. Phys. **80**, 4001 (1984).
[12] D. Babic, R. Tsu, and R. F. Greene, Phys. Rev. B **45**, 14 150 (1992).
[13] T. Takagahara, Phys. Rev. B **47**, 4569 (1993).
[14] G. Allan, C. Delerue, M. Lannoo, and E. Martin, Phys. Rev. B **52**, 11 982 (1995).
[15] M. Iwamatsu, M. Fujiwara, N. Happo, and K. Horii, J. Phys.: Condens. Matter **9**, 9881 (1997).
[16] P. G. Bolcatto and C. R. Proetto, Phys. Rev. B **59**, 12 487 (1999).
[17] L. Banyai, P. Gilliot, Y. Z. Hu, and S. W. Koch, Phys. Rev. B **45**, (1992).
[18] E. Rabini, B. Hetenyi, and B. J. Berne, J. Chem. Phys. **110**, 5355 (1999).
[19] P. Suppan and N. Ghoneim, *Solvatochromism* (The Royal Society of Chemistry, Cambridge, 1997).
[20] J. D. Simon, Acc. Chem. Res. **23**, 128 (1988).
[21] M. Quinten, J. Cluster Sci. **10**, 319 (1999).
[22] R. Elghanian, J. J. Storhoff, R. C. Mucic, and C. A. Mirkin, Science **277**, 1078 (1997).
[23] T. Vossmeyer, L. Katsikas, M. Giersig, I. G. Popovic, K. Diesner, A. Chemseddine, A. Eychmuller, and H. Weller, J. Phys. Chem. **98**, 7665 (1994).
[24] C. R. Kagan, C. B. Murray, and M. G. Bawendi, in *Microcrystalline and Nanocrystalline Semiconductors*, edited by L. Brus, M. Hirose, R. W. Collins, F. Koch, and C. C. Tsai, MRS Symposia Proceedings No. 358 (Materials Research Society, Boston, 1995), p. 219.
[25] M. V. Artemyev, A. I. Bibik, L. I. Gurinovich, S. V. Gaponenko, and U. Woggon, Phys. Rev. B **60**, 1504 (1999).
[26] C. B. Murray, D. J. Norris, and M. G. Bawendi, J. Am. Chem. Soc. **115**, 8706 (1993).

[27] C. B. Murray, C. R. Kagan, and M. G. Bawendi, Science **270**, 1335 (1995).

[28] In spherical QD's, electron states are labeled as *nL*, where $L=S,P,D$, etc., is the atomiclike notation for the angular momentum of the envelope wave function and *n* is the number of the state of a given symmetry. The subscript indicates the total angular momentum including the Bloch function momentum.

[29] C. R. Kagan, C. B. Murray, and M. G. Bawendi, Phys. Rev. B **54**, 8633 (1996).

[30] D. R. Lide, *CRC Handbook of Chemistry and Physics* (CRC Press, New York, 1999).

[31] W. P. Wuelfing, A. C. Templeton, J. F. Hicks, and R. W. Murray, Anal. Chem. **71**, 4069 (1999).

[32] Note that in the fits of Figs. 2 and 3, we plot the change in energy (Δ) of the exciton with respect to the value in hexane dispersion, not the absolute value of the polarization energy. As a result, the theoretical curves for different shell thicknesses only cross for $\varepsilon_3=1.89$ (hexane) and not when $\varepsilon_2=\varepsilon_3$ as one would intuitively expect.